Electron–ion coincidence measurements: The neutral dissociation plus excitation cross section for N_2

L. Mi and R. A. Bonham
Department of Biological, Chemical, and Physical Sciences, Illinois Institute of Technology, Chicago, Illinois 60616

(Received 4 December 1996; accepted 24 October 1997)

Pulsed electron beam time-of-flight measurements of the electron energy loss spectrum of molecular nitrogen at scattering angles of 28°, 45°, 71°, 112°, and 135° were made at impact energies of 24.5, 33.1, and 33.6 eV in coincidence with positive ions. The angular-dependent elastic, total inelastic, ionization, and neutral dissociation plus excitation cross sections were measured. The data were integrated over electron energy loss for each scattering angle. These angular-dependent data were then fitted with smooth analytic functions and integrated over angle to obtain individual total cross sections. All cross-section data were placed on an absolute scale by matching to total cross-section measurements reported in the literature. The angular-dependent elastic cross section and the integrated cross sections for elastic and total inelastic scattering were found to be in good agreement with literature values. Values obtained for the neutral dissociation plus excitation cross section agree with the sum of previous separate measurements of neutral dissociation and excitation. The total ionization cross sections are in fair agreement with accurate values reported in the literature. © *1998 American Institute of Physics.* [S0021-9606(98)01805-4]

I. INTRODUCTION

In the compilation of cross-section data bases required for modeling industrial process plasmas, a key cross section is the electron impact neutral dissociation cross section (i.e., dissociation of a molecule in to neutral fragments only).[1] So far only two direct methods[2,3] and two indirect methods[4,5] for measuring it have been reported. This paper presents a new indirect method for obtaining information on this important quantity.

A pulsed electron beam time-of-flight experiment is reported in which five electron impact energy loss spectra, all at different scattering angles, were recorded simultaneously and in coincidence with all positive ions produced in the experiment. The data can be used to determine the angular dependence of total, elastic, total inelastic, ionization (total and partial), and the sum of neutral dissociation and excitation cross sections. By use of appropriate analytic functions the angular scattering data for each cross-section type can be integrated over angle and energy loss to obtain the corresponding integrated cross section.

II. EXPERIMENT

A. Method

An abbreviated version of this experiment has been published in which a single detector for electrons was employed to measure an electron energy loss spectrum at a fixed scattering angle in coincidence with all ions produced.[5] The aim of that experiment was to measure an absolute instrumental ion detection efficiency for the apparatus used in our laboratory. In the process of carrying out that experiment we realized that it could also be used to measure the sum of neutral dissociation and excitation cross sections providing that the angular dependence of the scattering was also measured. The basic details of the experiment have been described elsewhere.[5,6] The novel aspect of the present experiment was the addition of four electron detectors to the experiment described in Ref. 5. The five time-of-flight electron detectors were placed at scattering angles of 28°, 45°, 71°, 112°, and 135° with ion detectors on each side of the plane containing the electron detectors. Figures 1 and 2 depict the apparatus configuration. The ion detection system has been described elsewhere[7] so only the details of the new electron detectors will be presented here.

Each electron flight tube had a detection solid angle of 3.5×10^{-3} sr (half angle of 2°) and a length of 27 cm. It used two 18-mm-diam microchannel plates in a chevron configuration to register electrons. The angles were measured to an accuracy of about 0.5° but a relative scale calibration procedure was employed which largely circumvented this source of uncertainty. The electron–ion coincidence data were used to establish the instrumental efficiency for ion detection for each electron detector. A typical spectrum is shown in Fig. 3, and an example of the instrumental efficiency, $\varepsilon(t)$, for one of the ion detectors is shown in Fig. 4. Efficiencies observed in this work were found to be about a factor of 2 smaller than values observed in our laboratory previously. We believe this may be due to aging of the ion detectors. In principle, the efficiency should be the same for each detector but differences were observed, especially for the 28° detector which had a higher count rate from electrons scattered from apertures and the chamber walls, and hence a lower efficiency for ion detection. Table I contains values for the detection efficiency for ions for the five electron detectors. Because there can be slight differences in the viewing solid angle of each detector and in the angular alignment, there is no guarantee that each detector sees a predictable region of the scattering volume. This means that the usually used angular-dependent

 0021-9606/98/108(5)/1904/6/$15.00

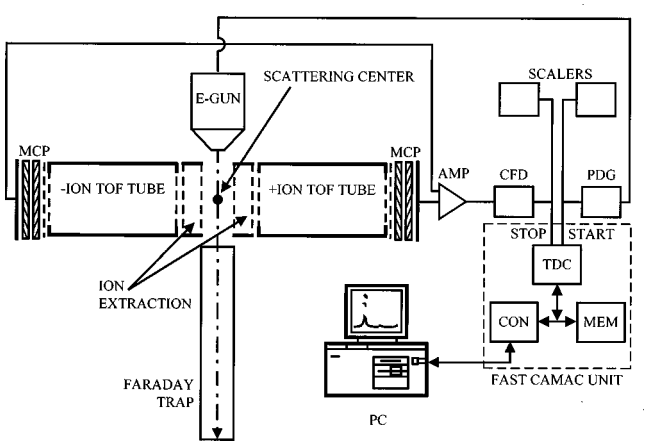

FIG. 1. Cross-sectional view of the apparatus showing the ion detectors with a block diagram of the data collecting electronics. The detectors for electrons, lie in a plane perpendicular to this figure, and are shown in Fig. 2.

corrections for placing data collected at different scattering angles on the same relative intensity scale[8] cannot be trusted. To circumvent this problem, we collected data for He at incident energies of 25, 30, and 50 eV and used the experimental data of Brunger *et al.*[9] to obtain a matching constant for each scattering angle. The fact that the matching constants were relatively independent of electron impact energy, as shown in Table II, was taken as validation of the procedure. Note that all the results at 45° have been normalized to unity and that the row labeled $\sin^2\theta$ corresponds to the reciprocal of the width of a viewing region, in and parallel to the electron beam, of the detector, assuming an infinitely narrow electron beam and a gas beam of uniform density over the observation distance *and assuming that all detectors have exactly the same solid angle of acceptance*. Clearly the acceptance solid angles of the detectors are not the same.

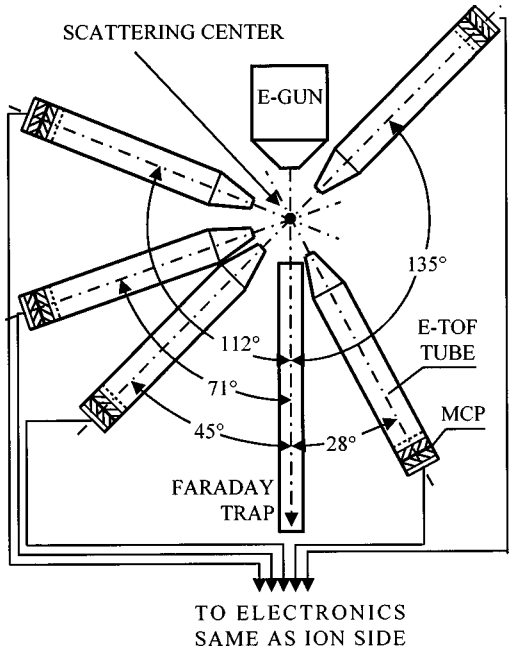

FIG. 2. Cross-sectional view of the apparatus showing the position of the five electron detectors. The plane of this view is perpendicular to the view shown in Fig. 1.

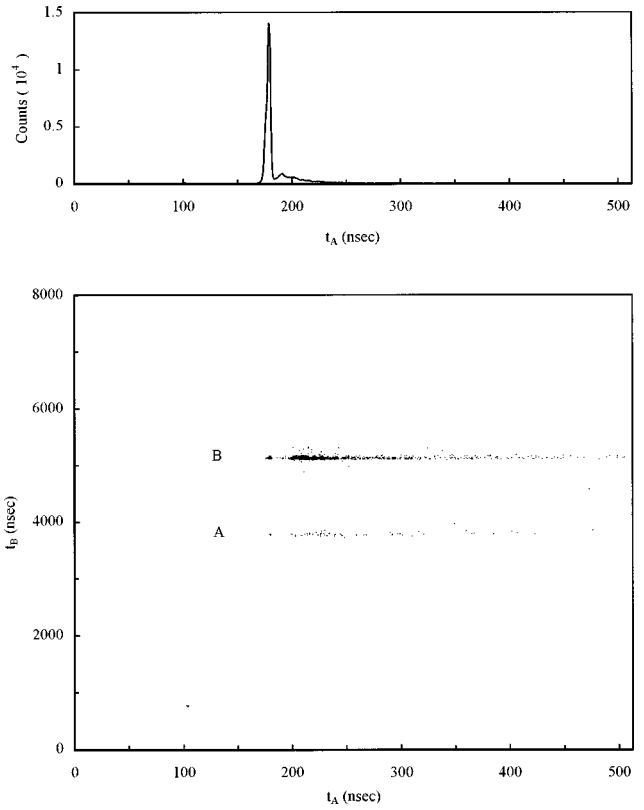

FIG. 3. Typical electron–ion coincidence and electron energy loss spectra. These spectra were recorded at a scattering angle of 135° and electron impact energy of 33.6 eV. The upper figure is the electron energy loss spectrum with total counts on the vertical axis and electron flight time on the horizontal axis. The dominant sharp peak is the elastic line while the weak features to its right constitute the inelastic scattering. The lower figure is a plot of the ion flight time on the vertical axis and electron flight time on the horizontal axis for electron–ion coincident events. The line labeled A corresponds to the partial ionization channel $e+N_2\rightarrow 2e+N+N^+$ while B labels the partial ionization channel $e+N_2\rightarrow 2e+N_2^+$. Accidental coincidences have been estimated and have been subtracted out.

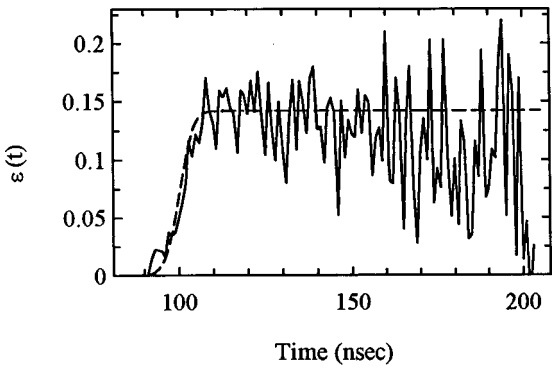

FIG. 4. The ion detection efficiency, $\varepsilon(t)$, as a function of electron flight time for the detector at 45° and an electron impact energy of 33.6 eV. The increasing noise with increasing electron flight time is due to increasing statistical uncertainty from the decreasing number of observed events. The smooth dashed curve is the theoretical efficiency based on the deconvolution procedure in Ref. 5.

TABLE I. Detector efficiencies.

Scattering angle	28°	45°	71°	112°	135°
Efficiency	0.06	0.14	0.15	0.17	0.15

In the case of the angular-dependent low energy limit of elastic scattering, a superposition of Legendre polynomials of the form

$$\left(\frac{d\sigma}{d\Omega}\right)_{\text{elastic}} = \sum_{i=0}^{4} a_i P_i(\cos\,\theta) \tag{1}$$

was employed to fit the data, which yielded integrated cross sections:

$$\sigma_{\text{elastic}} = 2\pi \int_0^{\pi} d\theta\, \sin\,\theta \left(\frac{d\sigma}{d\Omega}\right)_{\text{elastic}} = 4\pi a_0 . \tag{2}$$

Note that $\sin\theta$ in the definition of the integrated cross section acts as a weighting function which reduces the influence of both small ($\sim 0°$) and large angle ($\sim 180°$) data. The mathematical reason for using Legendre polynomials is that, for a central potential, the exact solution for the Schrödinger equation can be cast in the form of Legendre polynomials, and the coefficients in the Legendre function expansion are linearly independent. The physical reason is that for such a potential, angular momentum is conserved, and the Legendre polynomials are the eigenfunction of the angular momentum. Hence Legendre polynomials appear to be an obvious choice. With only five measurements, the integrals are sensitive to the choice of fitting functions. We tested the sensitivity of the present total elastic cross sections to the form of fit by repeating the procedure using the shape of the extensive experimental data of Shyn and Carignan[10] as a guide. The sensitivity test fitting function used was

$$\left(\frac{d\sigma}{d\Omega}\right)_{\text{elastic}} = b_0 + b_1\theta^{0.5} + b_2\theta^{0.75} + b_3\theta^{1} + b_4\theta^{1.25}. \tag{3}$$

For the elastic integrated cross section, the two different fits showed an agreement of 10% with that of Shyn and Carignan. An example of the result at the impact energy of 24.5 eV is presented in Fig. 5, where the solid curve is the Legendre fit and the dashed curve is the fit following Eq. (3). Since the elastic scattering dominates the total scattering, these same forms were used to fit the total scattering cross sections.

In the case of the inelastic cross sections, we chose to break up the cross section for any excitation *not resulting in ionization of the parent or a fragment* in to two parts. The cross section for any process which results in dissociation in to neutral fragments only will be referred to as the neutral dissociation cross section, while the cross section for excitation not resulting in dissociation will be called the excitation cross section. In the case of N_2, the processes are not separated in this experiment but have been in others.[2–4] The reason for this, perhaps cumbersome, choice is that it is experimentally possible to make the distinction between the two cross sections and in some cases, CF_4 for example, the excitation cross section in the sense used here vanishes. Our usage is also common practice in the literature of low temperature plasma modeling.

TABLE II. Scale factors for setting the relative intensity scale.

Scattering angle	28°	45°	71°	112°	135°
25 eV	0.18	1.00	0.50	0.94	0.85
30 eV	0.16	1.00	0.45	0.90	0.90
50 eV	0.18	1.00	0.40	1.04	0.84
$\sin^2\theta$	0.44	1.00	1.78	1.72	1.00

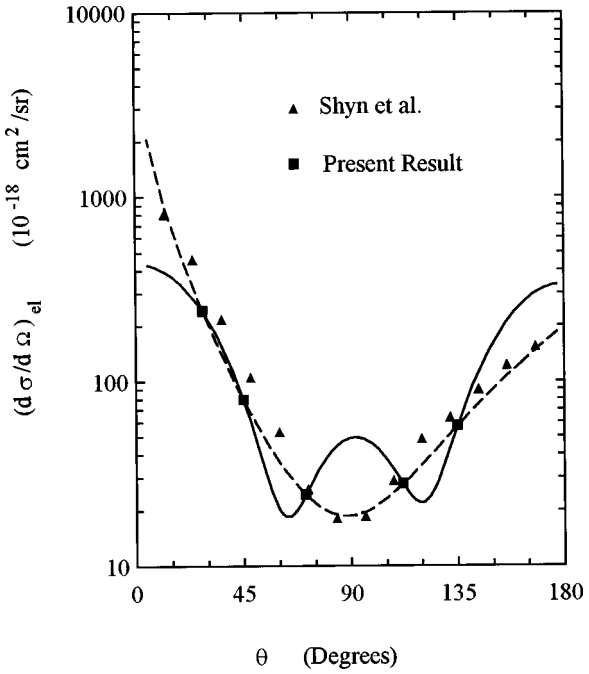

FIG. 5. The angular dependence of the elastic cross section for the electron impact energy of 24.5 eV. The triangles are values interpolated from the data of Shyn and Carignan, Ref. 10. The squares are the data points obtained in this study. The solid curve is the Legendre fit following Eq. (1) while the dashed curve is the fit following Eq. (3).

The determination of the angular dependence of the total inelastic, neutral dissociation plus excitation, and ionization contributions proved to be more difficult because of the paucity of our data and the absence of angular data from other laboratories (i.e., this is the first known attempt to measure these quantities). Our data were first transformed from a time-of-flight scale to an energy loss scale. The ionization contribution was placed on the same relative scale as the electron energy loss spectrum by means of the detector efficiency and subtracted out to obtain the relative contribution due to neutral dissociation plus excitation. A key assumption is that a region exists at sufficiently high energy loss where only ionization contributes to the inelastic scattering. This assumption was checked at an angle of 45° in the case of N_2 in Ref. 5 by collecting data on the rare gases. An example of results of this procedure for a single impact energy and scattering angle is shown in Fig. 6.

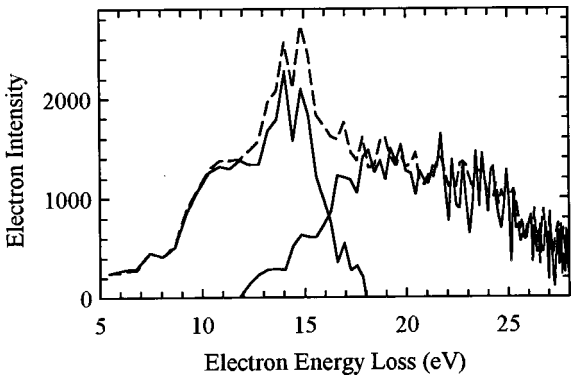

FIG. 6. A blow up of the inelastic portion of Fig. 3. The dotted curve is the total inelastic scattering while the solid curve on the right is the ion coincidence data which has been placed on the same scale by means of the ion detection efficiency. The solid curve on the left is the difference between the former two curves and represents the contribution from the sum of neutral dissociation and excitation.

These data were then integrated over energy loss and each of the three different data sets (total inelastic, ionization, and neutral dissociation plus excitation) were then fitted to an expansion in Legendre polynomials of the form

$$\left(\frac{d\sigma}{d\Omega}\right)_{\text{inelastic}} = a_0 P_0(\cos\,\theta) + \sum_{n=1}^{N} a_{j_n} P_{j_n}(\cos\,\theta) \qquad (4)$$

to get the individual integrated cross sections. To test the sensitivity of the integrated cross section to the choice of Legendre expansion, we repeated the fitting procedure with $N=2$, 3, or 4 and the order of Legendre functions, j_n, varied over the range from 1 to 10. Only those least-squares fits to the experimental data which yielded a R-squared value larger than 0.95 and had positive definite cross sections (''good'' fits) were considered as candidates for estimating the integrated cross sections. Such a fitting choice is dictated by the fact that, for a central potential, as the impact energy is lowered, the number of significant terms of Legendre polynomials needed in the expansion of the angular dependence of the wave function decreases. The integrated cross sections, $\sigma_{\text{inelastic}}$, σ_{ion}, or $\sigma_{\text{neut.dissoc}}$, are given by the simple formula $4\pi a_0$ in all cases. All ''good'' fits were found to contain P_0, P_2, and P_4 terms. Typically the coefficients of these three terms were quite stable and were much bigger than those of other terms in the cases of four- ($N=3$) and five-term ($N=4$) fits. In fact, the deviation from the average integrated cross section of all fits was less than 10%. Table III shows the coefficients a_0, a_2, and a_4 of the three-term fits (P_0, P_2, P_4). Typical results of angular fits to the data for ionization at 33.1 eV are shown in Fig. 7, those for neutral dissociation plus excitation at 33.6 eV are shown in Fig. 8.

Since the total inelastic cross section is the sum of the ionization cross section and the neutral dissociation plus excitation cross section, the consistency of the inelastic data could be tested (i.e., does the sum of angle integrated ionization and neutral dissociation plus excitation equal the angle integrated sum of the two?). Table IV shows the comparison

TABLE III. Coefficients a_i of three-term Legendre fits (P_0,P_2,P_4) (unit: 10^{-18} cm^2/sr).

Process	Energy (eV)	a_0	a_2	a_4
Neutral dissociation plus excitation	24.5	15.23	13.26	27.29
	33.1	17.40	30.95	38.64
	33.6	18.33	34.67	46.32
Ionization	24.5	5.50	7.76	13.95
	33.1	8.17	12.02	19.41
	33.6	8.74	12.16	21.24
Total inelastic	24.5	22.65	31.63	53.96
	33.1	25.28	42.74	57.75
	33.6	27.07	46.83	67.56
Elastic	24.5	87.91	211.25	168.08
	33.1	81.22	197.77	195.36
	33.6	79.07	190.79	181.05

of the sum of the ionization and neutral dissociation plus excitation cross sections with the directly determined total inelastic cross section.

B. Normalization to an absolute scale

Experimental values obtained by others are available for the total,[11] integrated elastic,[10] and integrated ionization cross sections.[12,13] The question is which to use for normalizing the experimental data? The total and integrated ionization cross sections are most accurately determined, but, because the detection efficiency for very low energy elec-

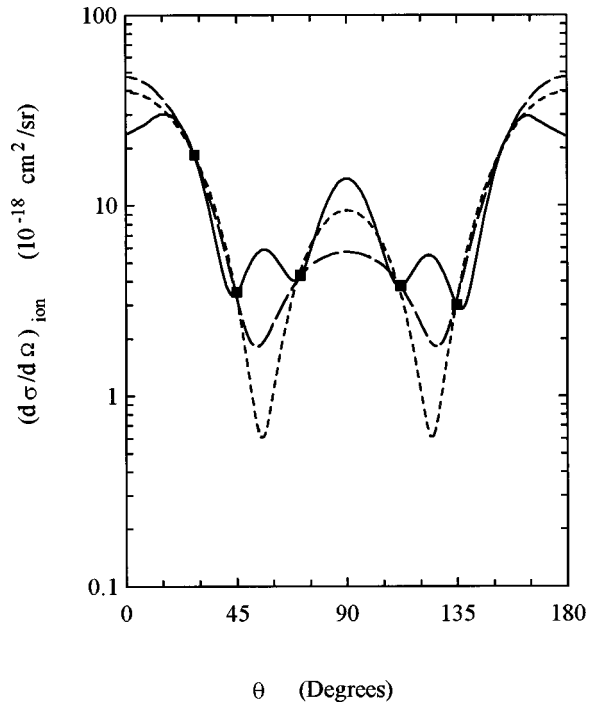

FIG. 7. The angular dependence of scattered electrons producing ionization at 33.1 eV. The solid curve is a representative five-term Legendre fit (P_0,P_1,P_2,P_4,P_{10}), the long dashed curve is a representative four-term Legendre fit (P_0,P_2,P_4,P_6), and the short dashed curve is the three-term fit (P_0,P_2,P_4).

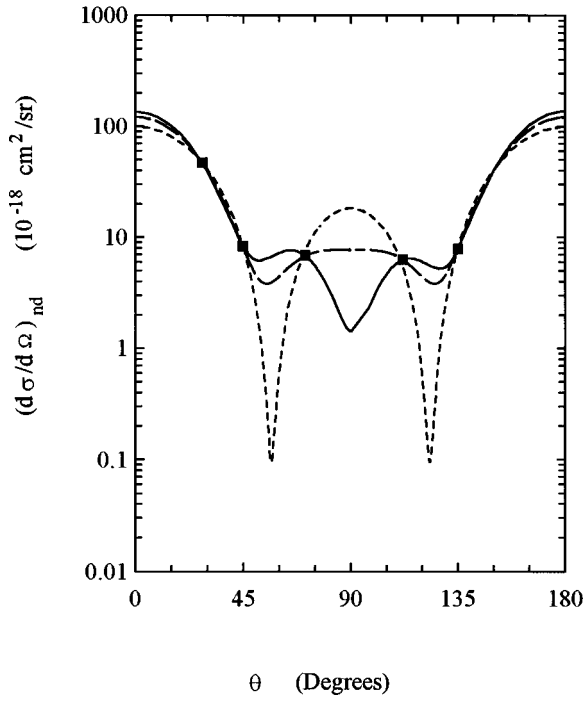

FIG. 8. The angular dependence of electrons producing neutral dissociation plus excitation at 33.6 eV. The solid curve is a representative five-term Legendre fit (P_0,P_2,P_3,P_4,P_6), the long dashed curve is a representative four-term Legendre fit (P_0,P_2,P_4,P_6), and the short dashed curve is the three-term fit (P_0,P_2,P_4).

trons can be expected to decrease to zero due to surface charging in the apparatus it is expected that the ionization contribution to the spectrum will be systematically too small. Normalizing on the ionization cross section would then result in a neutral dissociation plus excitation cross section that was too large. A bigger problem is that the region of energy loss corresponding to ionization has the highest statistical uncertainty and hence the largest random error. The best available literature values for the integrated elastic cross section, unlike those available for the ionization and total cross sections which have 3%–5% uncertainties, are uncertain by 10%–15%. Hence, we chose Kennerly's total cross-section results,[11] which are 3% accurate, for normalization of our data. The previously mentioned uncertainties in our ionization cross-section measurements do not affect the total cross section in a major way since the integrated ionization cross section is less than 10% of the total cross section (i.e., a 30% error in the ionization cross section translates to a less than 3% error in the total).

TABLE IV. Comparison of integrated cross sections obtained from various polynomial fits (unit: 10^{-16} cm^2).

Process	Energy (eV)	Four-term fits	Five-term fits
Neutral dissociation plus excitation	24.5	1.95±0.09	1.89±0.17
	33.1	2.19±0.05	2.17±0.08
	33.6	2.22±0.22	2.12±0.19
ionization	24.5	0.69±0.04	0.71±0.03
	33.1	1.02±0.08	1.00±0.09
	33.6	1.07±0.03	1.08±0.02
Total inelastic	24.5	2.80±0.27	2.73±0.16
	33.1	3.12±0.14	3.17±0.15
	33.6	3.30±0.32	3.19±0.22

III. RESULTS AND CONCLUSIONS

In Fig. 3 a typical coincidence spectrum, taken at an angle of 135° and an impact energy of 33.6 eV, is shown. The electron impact energy loss spectrum is displayed at the top with the ions in coincidence recorded below. Accidental coincidences have been subtracted from the spectrum and the horizontal coincidence line labeled A corresponds to N^+ and B to N_2^+. In Fig. 4 the ratio of total ion coincidence counts to total electron counts is shown as a function of electron flight time (energy loss) for 33.6 eV incident electrons scattered through 45°. This ratio corresponds to the absolute instrumental efficiency for ion detection. The increasing noise for long electron flight times is due to a large statistical uncertainty from the low number of events registered. The smooth dashed curve is the theoretical efficiency based on the deconvolution procedure in Ref. 5. The matching scale factor for this theoretical curve, the instrumental efficiency, has been determined by least-squares fitting to the experimental data. Figure 6 shows a blown up portion of the inelastic energy loss spectrum shown in Fig. 3 plotted as a function of energy loss. Note that the intensity obtained by time of flight, $d\sigma/dt$, requires multiplication by the cube of the flight time for conversion to $d\sigma/dE$. The ionization contribution, obtained from the coincidence spectrum, has been placed on the same relative scale by means of the instrumental efficiency. Subtraction of the ionization from the total inelastic reveals the contributions from excitation and neutral dissociation. To obtain the total ionization cross section the apparent total ionization cross section (the number of e–ion coincident events) must be divided by two since the ionization region includes both scattered and ejected electrons. The dividing factor could be somewhat larger than two if cross sections for multiple charge ionization were appreciable in comparison to the single ionization cross sections, which is not the case here because of the low impact energies used.

The coefficients, a_i, of three-term Legendre fits (P_0,P_2,P_4) for various angular-dependent cross sections are given in Table III. Since the P_0, P_2, and P_4 terms dominated in the four- and five-term Legendre fits, and the coefficients of these three terms were found to be relatively constant, the coefficients for four- and five-term Legendre expansions are not included in Table III. The results from fitting the angular differential cross sections to various four- and five-term Legendre functions are given in Table IV. The uncertainties are the standard deviation of all fitting results. Additional uncertainties are discussed below. It is obvious that the integrated cross sections are relatively independent of the fit and that the sum of neutral dissociation plus excitation and the ionization cross sections add up to the total inelastic cross section in each case. In order to extract the neutral dissociation cross section we have added up the in-

TABLE V. Excitation cross sections given by Itikawa *et al.* (unit: 10^{-16} cm^2).

State	24.5 eV	33.4 eV
$a''\ ^1\Sigma_g^+$	0.045	0.018
$b'\ ^1\Sigma_u^+$	0.110	0.088
$c'\ ^1\Sigma_u^+$	0.050	0.100
$a'\ ^1\Sigma_u^-$	0.032	0.019
$E\ ^3\Sigma_g^+$	0.005	0.003
$A\ ^3\Sigma_u^+$	0.091	0.053
$B'\ ^3\Sigma_u^-$	0.036	0.029
$a\ ^1\Pi_g$	0.260	0.180
$b\ ^1\Pi_u$	0.220	0.220
$c\ ^1\Pi_u$	0.090	0.083
$o\ ^1\Pi_u$	0.022	0.020
$B\ ^3\Pi_g$	0.100	0.075
$C\ ^3\Pi_u$	0.100	0.050
$F\ ^3\Pi_u$	0.017	0.016
$G\ ^3\Pi_u$	0.026	0.020
$w\ ^1\Delta_u$	0.025	0.013
$W\ ^3\Delta_u$	0.170	0.060
Total	1.399	1.047

dividual excitation cross sections given by Itikawa *et al.*[14] The results shown in Table V were obtained from Ref. 14 by linear interpolation and extrapolation being careful to only use measured excitation cross sections in order to avoid cascade corrections present in emission cross section measurements.

In Table VI the results obtained in this study are compared to those obtained by other investigators. Note that we have averaged our results obtained at 33.1 and 33.6 eV and report the results at the average of the two energies. The estimated uncertainties in our results take into account the uncertainties in the normalizing data (N_2 total cross section and He elastic cross sections), statistical uncertainty from number of events observed, estimated uncertainty in determining the detector efficiencies, and the uncertainty introduced by the use of different fitting functions to obtain integrated cross sections.

In Table VI, the ''present result'' for ''neutral dissociation'' is the difference between our measurement and our estimate of excitation derived from the data given in Ref. 14.

TABLE VI. Comparison of integrated cross-section measurements by different investigators (unit: 10^{-16} cm^2).

Process	Reference	24.5 eV	33.4 eV
	Present result	0.52±0.27	1.15±0.22
Neutral Dissociation	4–13	1.0±0.2	1.4±0.3
	2	0.70±0.22	0.84±0.27
	2+4	0.81±0.18	1.08±0.22
Ionization	Present result	0.70±0.18	1.05±0.17
	13	0.54±0.02	1.20±0.04
Excitation	14	1.40±0.11	1.05±0.09
Total Inelastic	Present result	2.79±0.42	3.23±0.29
	2+13+14	2.75±0.21	3.33±0.24

The uncertainties for our estimates of the excitation cross sections were based on the uncertainties of individual excitation cross sections and did not take into account the fact that some cross sections assigned to excitation might actually belong to dissociation. The entry ''4−13'' for ''neutral dissociation'' means the total dissociation results of Winters[4] with the dissociative ionization given in Ref. 13 subtracted out. The entry ''2+4'' for ''neutral dissociation'' is the best estimate, combining the results of direct measurement of neutral dissociation of Cosby with that of Winters, given by Cosby in Ref. 2. The entry ''2+13+14'' for ''total inelastic'' denotes the sum of Cosby's neutral dissociation result, our estimate of excitation, and the new highly accurate measurements of the total ionization.

The most accurately determined inelastic cross sections in our experiments are the total inelastic and the sum of neutral dissociation plus excitation cross sections. This is because of the large uncertainty in determination of the ionization contribution at high energy loss (small scattered electron energy). Unfortunately, molecular nitrogen is not an ideal test case because the uncertainties in the existing measurements of excitation cross sections contributed considerable uncertainty to our neutral dissociation cross-section results. The best we can do is to accept the values for the neutral dissociation cross section given in Ref. 2 and subtract these values from our measurements to obtain an estimate of the total excitation cross section. Such a procedure yields results in good agreement with the sum of all measured excitation cross sections given in Ref. 14. The total ionization cross section is in agreement with the accurate measurements reported in Ref. 13 to within our error estimate.

In summary, we have reported a new indirect method for determining the sum of integrated cross sections for neutral dissociation and excitation. The results are in agreement with previously published estimates for these quantities and serve as a calibration of the technique. The agreement obtained here should pave the way for the use of this technique to settle a dispute as to the correct neutral dissociation cross section for the important etching gas CF_4 for which the excitation cross section vanishes at all electron impact energies. These results will be reported in a forthcoming paper.

[1] R. A. Bonham, Jpn. J. Appl. Phys., Part 1 **33**, 4157 (1994).
[2] P. C. Cosby, J. Chem. Phys. **98**, 9544 (1993).
[3] T. Nakano, H. Toyoda, and H. Sugai, Jpn. J. Appl. Phys., Part 1 **31**, 2919 (1992).
[4] H. F. Winters, J. Chem. Phys. **44**, 1472 (1966).
[5] M. R. Bruce and R. A. Bonham, J. Mol. Struct. **352/353**, 235 (1995).
[6] M. R. Bruce, L. Mi, C. R. Sporleder, and R. A. Bonham, J. Phys. B **27**, 5773 (1994).
[7] Ce Ma, M. R. Bruce, and R. A. Bonham, Phys. Rev. A **44**, 2921 (1991).
[8] H. F. Wellenstein, H. Schmoranzer, R. A. Bonham, T. C. Wong, and J. S. Lee, Rev. Sci. Instrum. **46**, 92 (1975).
[9] M. J. Brunger, S. J. Buckman, L. J. Allen, I. E. McCarthy, and K. Ratnavelu, J. Phys. B **25**, 1823 (1992).
[10] T. W. Shyn and G. R. Carignan, Phys. Rev. A **22**, 923 (1980).
[11] R. E. Kennerly, Phys. Rev. A **21**, 1876 (1980).
[12] D. Rapp and P. Englander-Golden, J. Chem. Phys. **43**, 1464 (1965).
[13] H. C. Straub, P. Renault, B. G. Lindsay, K. A. Smith, and R. F. Stebbings, Phys. Rev. A **54**, 2146 (1996).
[14] Y. Itikawa, M. Hayashi, A. Ichimura, K. Onda, K. Sakimoto, K. Takayanagi, M. Nakamura, H. Nishimura, and T. Takayanagi, J. Phys. Chem. Ref. Data **15,** 985 (1986).